Food Chemistry: X 21 (2024) 101237

Contents lists available at ScienceDirect

Food Chemistry: X

journal homepage: www.sciencedirect.com/journal/food-chemistry-x

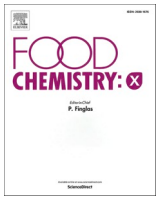

Fabrication of diosmin loaded food-grade bilayer nanoparticles with modified chitosan and soy peptides and antioxidant properties examination

Sen Li [a,b], Tong Guan [a,b], Hongyan Lv [a,b], Yuwei Cai [a,b], Wanqing Cao [a,b], Ze Zhang [a,b], Hongdong Song [a,b], Hongwei Cao [a,b], Xiao Guan [a,b,*]

[a] School of Health Science and Engineering, University of Shanghai for Science and Technology, Shanghai 200093, China
[b] National Grain Industry (Urban Grain and Oil Security) Technology Innovation Center, Shanghai 200093, China

ARTICLE INFO

Keywords:
Diosmin
Nanoparticles
Antioxidant activity
Soy peptides
Trimethyl chitosan

ABSTRACT

Diosmin is a flavonoid derived from plants, possessing anti-inflammatory, antioxidant, antidiabetic, neuroprotective and cardiovascular protective properties. However, diosmin has low solubility in water, leading to low bioavailability. In this study, we constructed bilayer nanoparticles with trimethyl chitosan and soy peptides to improve the oral bioaccessibility and bioavailability of diosmin, and determined the characteristics and antioxidant properties of the diosmin-loaded nanoparticles. The results showed that the size of the nanoparticles was around 250 nm with the encapsulation efficiency higher than 97 %, and the nanoparticles were stable under regular conditions. *In vitro* digestion suggested the nanoparticles could protect diosmin from releasing in gastric digestion but promote the bioaccessibility of diosmin in intestine. Furthermore, the diosmin-loaded nanoparticles presented excellent antioxidant activities *in vitro* and significantly decreased the Lipopolysaccharides-induced brain Malondialdehyde (MDA) level by oral administration. Therefore, the reported nanoparticles may be an effective platform for improving the oral bioavailability of diosmin.

1. Introduction

As a flavonoid, the pharmacological activity of diosmin (Chemical structure shown in Fig. 1) has been reported by many studies. It was found to possess antioxidant (Wojnar, Kaczmarczyk-Sedlak, & Zych, 2017), anti-inflammatory (Berkoz, 2019), anti-diabetes(Hsu, Lin, Cheng, & Wu, 2017), anti-cancer (Naso et al., 2016), anti-microbial (Pushkaran et al., 2019), neuroprotective (Carballo-Villalobos, González-Trujano, Pellicer, Alvarado-Vásquez, & López-Muñoz, 2018) and cardiovascular protective activities (Paredes et al., 2018). Among which, the anti-oxidant activity of diosmin is important, as oxidative stress is found to play an important role in the pathophysiology of many diseases. However, under natural conditions, most flavonoids exist as glycosides, which have low solubility in water and are not readily absorbed by gastrointestinal tract. Diosmin is almost insoluble in water and alcohol. After oral administration, diosmin is barely absorbed directly in small intestine. The application of diosmin is greatly limited due to its low water solubility and bioavailability.

Many efforts have been done to increase the water solubility and bioavailability of diosmin. Early trial is the administration of micronisation to reduce the obstruction of diosmin's intestinal absorption by particle size (Garner, Garner, Gregory, Whattam, Calam, & Leong, 2002). Russo et al. developed an μsmin®Plus buffer reagent formulation of diosmin using micronisation technique to further increase the bioavailability of diosmin in the systemic circulation in clinical trial studies (Russo, Chandradhara, & De Tommasi, 2018; Russo, Mancinelli, Ciccone, Terruzzi, Pisano, & Severino, 2015; Serra et al., 2021). Freeze-dried phospholipid complexes loaded with diosmin also exhibited

Abbreviations: TMC, trimethyl chitosan; SPI, soy protein isolate; SPA, soybean polypeptide aggregation; HSPA, heated soybean peptide aggregation; SPN-D, SPA nanoparticles containing diosmin; HSPN-D, HSPN nanoparticles containing diosmin; CSK-TMC, CSK conjugated trimethyl chitosan; CT-SPN-D, CSK conjugated trimethyl chitosan -coated SPN-D; CT-HSPN-D, CSK conjugated trimethyl chitosan -coated HSPN-D; TPP, tripolyphosphate; SDS, sodium dodecyl sulfate; DTT, DL-Dithiothreitol; DMEM, Dulbecco's modified Eagle medium; HBSS, Hank's balanced salt solution; LPS, lipopolysaccharide; MDA, malondialdehyde; PDI, polydispersity index; EE, encapsulation efficiency; GD, gastric digestion residues; GID, gastrointestinal digestion residue; SD, standard deviation; DLS, Dynamic Light Scattering; FTIR, Fourier transform infrared analysis; DSC, Differential Scanning Calorimeter; HPLC, High Performance Liquid Chromatography.

* Corresponding author at: School of Health Science and Engineering, University of Shanghai for Science and Technology, 516 Jungong Road, Shanghai 200093, China.
E-mail address: gnxo@163.com (X. Guan).

https://doi.org/10.1016/j.fochx.2024.101237
Received 9 January 2024; Received in revised form 14 February 2024; Accepted 15 February 2024
Available online 18 February 2024

improved drug dissolution and intestinal permeability (Freag, Elnaggar, & Abdallah, 2013). Anwer et al. converted a mixture of Soluplus® and diosmin mixed in an alkaline ethanol solution into a solid dispersion with enhanced solubility by spray drying (Anwer et al., 2020), and found the solid dispersion was more protective against thioacetamide-induced renal and hepatic injury compared to free diosmin.

Nano-technology shows promising prospect on the enhancement of the solubility and bioavailability of diosmin. Vrbata et al. prepared nanofibres loaded with diosmin using electrostatic spinning technique, and reported that the nanofibres not only improved the dissolution of diosmin *in vitro*, but also enhanced its absorption *in vivo* (Vrbata, Berka, Stránská, Doležal, & Lázníček, 2014). Hendawy et al. prepared polymeric nanoparticles loaded with diosmin by emulsion–solvent evaporation and acid–base neutralization. The nanoparticles could continuously control the release of diosmin and improve its bioavailability in the rat diabetes model (Om et al., 2020). Moriwaki et al. synthesized a diosmetin-7-glucoside-γ-cyclodextrin complex which showed high solubility, high bioavailability and short absorption time (Moriwaki et al., 2023). Other researchers have successfully constructed chitosan-coated PLGA nanocarriers to improve gastric retention and prolong diosmin release in rats (Abd El Hady, Mohamed, Soliman, & El-Sabbagh, 2019).

Food-originated embedding materials show advantages in the oral delivery of bioactive compounds. Soy protein is considered as an admirable raw material for the development of nanoparticles in the food industry. Amphiphilic soy peptides produced by the hydrolysis of soy protein isolate can self-assemble to form ordered nanostructures. Chitosan is also widely used in nanoparticle construction, as it is water-soluble, biocompatible, non-toxic. It shows strong permeability under acidic conditions to encapsulate bioactives in nanoparticle delivery systems (Y. C. Wang, Li, & Kong, 2013). In this study, we constructed double-layer nanoparticles by using soy peptides and trimethyl chitosan to improve the bioaccessibility and bioavailability diosmin. Diosmin was encapsulated by the self-assemble of soy peptides and then coated by trimethyl chitosan (TMC). A goblet cell-targeting CSK peptide was linked to the TMC to further promote the bioavailability of the nanoparticles. The basic physiochemical characteristics, stability, toxicity and antioxidant activity was determined.

2. Materials and methods

2.1. Animals

ICR mice (male, 6–8 weeks, 30–35 g) and SD rats (male, 200–250 g body weight) were purchased from Shanghai Jiesijie Laboratory Animal Co., Ltd. with a light–dark cycle of 12 h, free access to food and water, and consumed ordinary irradiation maintenance feed purchased from Jiangsu Xietong Pharmaceutical Bio-engineering Co., Ltd. Prior approval was obtained from the Ethics Committee of the University of Shanghai for Science and Technology in accordance with the Chinese Standards for Laboratory Animals, and all animal experiments were performed according to the National Institutes of Health guide for the

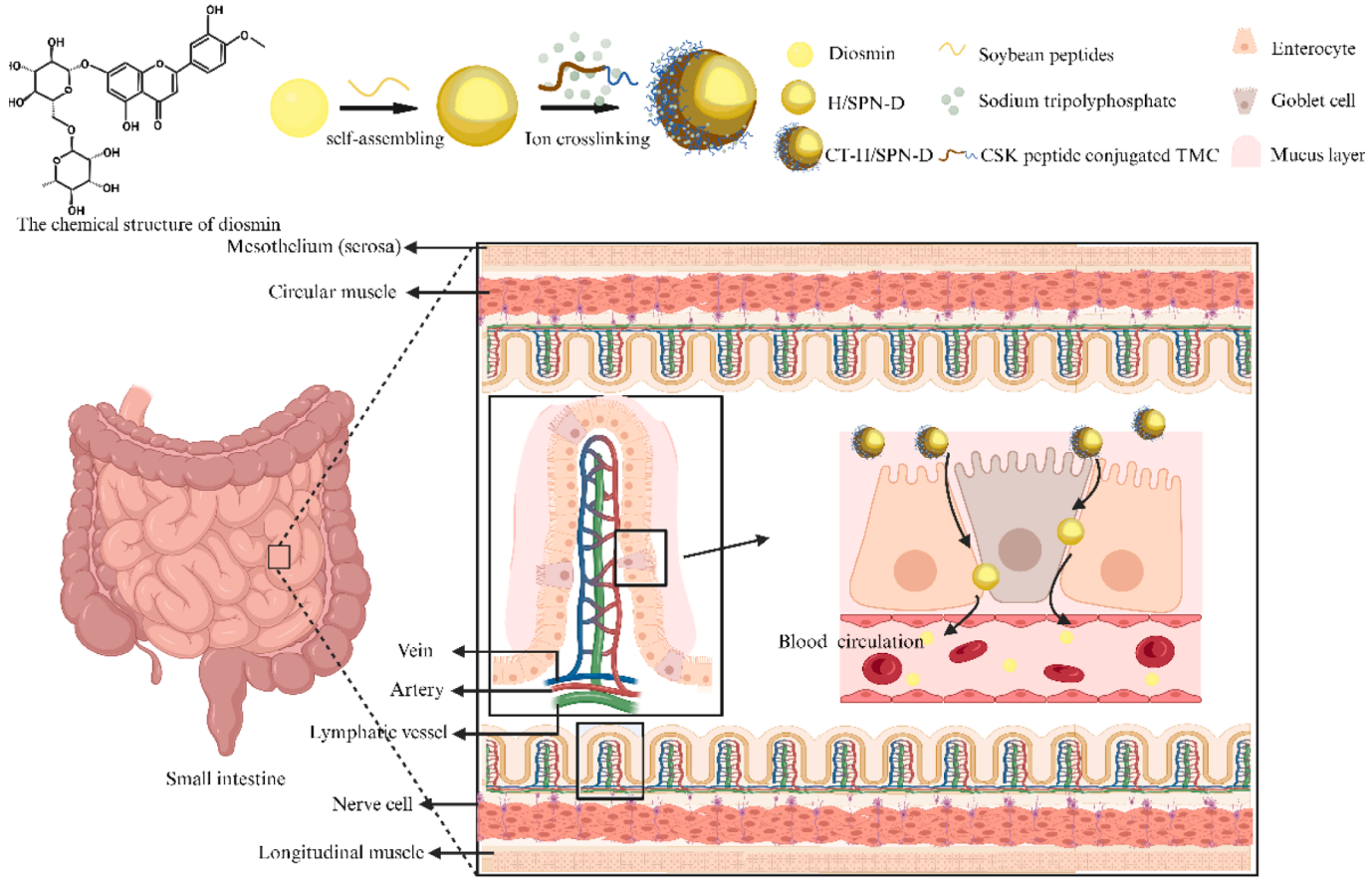

Figure 1 The construction scheme of the nanoparticles

Fig. 1. The construction scheme of the nanoparticles.

care and use of Laboratory animals (NIH Publications No. 8023, revised 1978).

2.2. Materials and chemicals

Diosmin (~95 % purity), soy protein isolate (SPI), chitosan (>95 % deacetylated, low viscosity 100–200 mPa.s), dimethylsulfate, 1-(3-Dimethylaminopropyl)-3-ethylcarbodiimide hydrochloride (EDC·HCl) and *N*-Hydroxysuccinimide (NHS) were purchased from Macklin Biochemical Co., Ltd (Shanghai, China). CSK peptide was purchased from GL Biochem Ltd (Shanghai, China). Alcalase (2.4 U/g; alkaline protease) was purchased from Sigma-Aldrich (St. Louis, Missouri, USA). All reagents were analysis grade.

2.3. Preparation of nanoparticles on basis of soybean peptides

Four gram of SPI was dissolved in 100 mL of deionized water, adjusting pH to about 8. The solution was enzymatically digested with alcalase (0.6 U/g protein) at 50 °C, with the pH kept constant (Zhang, Zhou, Zhao, Lin, Ning, & Sun, 2018). After digestion of the solution, the pH was reduced to 7.0. The precipitate was extracted by centrifugation at 8000 rpm for 20 min at 4 °C. The sediment was washed, centrifuged and freeze dried to get soybean polypeptide aggregation (SPA). Before centrifuging the solution, heated soybean peptide aggregation (HSPA) was obtained by heat inactivation under 90 °C for 30 min.

Freeze-dried SPA or HSPA was dissolved in 1 % (w / v) ultrapure water and stirred magnetically under 700 rpm for 2 h to obtain soybean polypeptide suspension. Diosmin was dissolved in 0.1 M NaOH to obtain diosmin alkali solution with a concentration of 100 μg/mL. During the magnetic stirring, diosmin alkali solution was quickly added into soybean polypeptide suspension at a volume ratio of 1:1. The pH of the mixture was adjusted to 7.0 after stirred for 30 min, and then the mixture was ultrasonic treated for 10 min (power 150 W, 5 s / 5 s on / off). Finally, after centrifugation (8000 rpm, 20 min), the supernatant was taken to obtain SPA nanoparticles containing diosmin (SPN-D) or HSPA nanoparticles containing diosmin (HSPN-D).

2.4. Fabrication of nanoparticles wrapped with CSK-TMC

The CSK conjugated TMC (CSK-TMC) was prepared as previously reported (Li et al., 2022). The 1.0 mg/mL sodium tripolyphosphate (TPP) solution and Tween 80 were mixed in a ratio (30:1, v / v). The preparation of SPN-D/HSPN-D was gradually added to the CSK-TMC solution at pH 5.5 (4:1, v / v). After the mixture was stabilized, the TPP/Tween80 mixture was slowly added at a ratio of 1:10 (v / v) with the CSK-TMC solution. Then, the blend was agitated at 700 rpm for 60 min to get nanoparticles CT-SPN-D/CT-HSPN-D.

2.5. Characterization of nanoparticles

Dynamic Light Scattering (DLS) (Nano ZS90 instrument, Malvern, Worcestershire, UK) was used to measure the particle size, polydispersity index (PDI) and Zeta potential of the diluted samples. All measurements were performed at 25 °C.

The sample was prepared by negative dying method to observe the surface morphology by using Transmission Electron Microscope (TEM-JEM2100, Jeol, Japan). Nanoparticles after 10 times dilution were dropped on a copper grid coated with formvar carbon. Then, the extra nanoparticles were absorbed following the solution was dispersed. After drying at room temperature, the copper added 1 % phosphotungstic acid and absorbed it as described above.

Storage stability of the nanoparticles was determined under room temperature at pH 7, pH 8 and pH 9. The zeta potential was determined after 1 day and 16 days respectively.

Various organic fluids were used to assay the interaction forces within nanoparticles by solvent-perturbation method. 6 M urea, 0.5 % sodium dodecyl sulfate (SDS), 30 mM DL-Dithiothreitol (DTT) solvents were prepared with ultrapure water at pH 7.0. These above solvents and distilled water, were used separate or mixed (Liu & Tang, 2014). The particle size was determined after the nanoparticles were well scattered in various organic solvents.

The Germany Brooke AXSD8 advanced diffractometer was used to analyze the XRD patterns of nanoparticles and mixtures. The instrument had a copper anode producing copper Kα X-rays ($\lambda = 0.15418$ nm) with an accelerating voltage of 40 kV and a tube current of 40 mA. The angular range was from 3° to 50° in steps of 0.02° at a scanning speed of 0.1 s/step.

Fourier transform infrared analysis (FTIR) was performed using a Nicolet Is50 Fourier transform infrared spectrometer (Thermo Fisher Scientific, USA). 5 mg of freeze-dried samples were mixed and ground with 200 mg of potassium bromide (KBr) and then dried under infrared light. The mixture was scanned 128 times with a resolution of 2 cm^{-1} in the range of 400 to 4000 cm^{-1} to get the infrared spectrum of samples.

Differential scanning calorimetry was performed using a Q2000 Differential Scanning Calorimeter (DSC) from TA company, USA. The nitrogen flow rate of the sample was set to 40 mL/min at 10 °C /min in the range of 25 °C to 300 °C.

2.6. Encapsulation efficiency (EE)

According to the following equation to calculate the EE (%):

$$\mathrm{EE}(\%) = encapsulateddiosmin(mg)/initialdiosmin(mg) \times 100$$

where diosmin that was loaded in the nanoparticles was taken by anhydrous methanol extraction. The diosmin content of nanoparticles was assayed by High Performance Liquid Chromatography (HPLC).

The calculation of diosmin concentration in encapsulation based on EE:

$$C_{diosmin} = diosminquality(m_0)/watervolume(V_0)*EE$$

where m_0 denoted the diosmin's initial mass and V_0 denoted the volume of water used in the nanoparticle formation process.

2.7. In vitro digestion and ex vivo absorption of nanoparticles

In vitro gastrointestinal digestion and *ex vivo* absorption experiments were slightly modified based on previous reports (Campos-Vega, Vázquez-Sánchez, López-Barrera, Loarca-Piña, Mendoza-Díaz, & Oomah, 2015). During the gastric digestion stage, 5 mL of prepared nanoparticles solution was regulated pH to 1.5–2.0, 1.6 mg of pepsin was added. The mixture was shaken in a water bath at 37 °C for 2 h. Then, the mixture was adjusted to pH 7.0, and treated as gastric digestion residues (GD). During enteric digestion, 1.6 mg trypsin was added to GD. The mixture was shaken in a water bath at 37 °C for 2 h and considered as gastrointestinal digestion residue (GID). The supernatant was centrifuged at 10,000 × g for 10 min, and then centrifuged at 12,000 rpm for 10 min in an ultrafiltration centrifuge tube (100 K_D) to filter the GD and GID to obtain the diosmin released from the nanoparticles. The filtrate was analyzed by HPLC. The release rate (%) of diosmin was calculated according to the below formula:

$$\text{Release rate}\,(\%) = C_{freediosmin}/C_{NPs} \times 100$$

where $C_{\text{free diosmin}}$ was the concentration of free diosmin in the digestion residues, C_{NPs} was the concentration of diosmin in nanoparticles.

In terms of *ex vivo* absorption of nanoparticles, SD rats (male, 200–250 g body weight) were taken and fasted overnight, and then executed by intraperitoneal injection of excess chloral hydrate (1000 mg/kg body weight) on the day of the experiment; the upper end of the duodenum and the lower end of the ileum were resected immediately after the execution, and the ileocecal intestinal segments were taken.

The intestinal sacs were washed with Ringer's solution, appropriate amount of NPs or free diosmin solution was added, and the ends were ligated, then put into a centrifuge tube filled with 5 mL of Ringer's solution, and shaken in a 37 °C water bath. 0.5 mL of the sample was extracted from the centrifuge tube at the 20, 40, 60, 80, 100 and 120 min, 0.5 mL of Ringer's solution was put. The samples were analyzed by HPLC after filtration through a 0.45 μm filter membrane. Experiments were performed three times and all results were subjected to *t*-test ($p < 0.05$). The calculation of the bioaccessibility (%) of diosmin is used by the below formula:

$$\text{Bioaccessibility}\ (\%) = C_t / C_{NPs} \times 100$$

where C_t was the concentration of diosmin crossing the intestinal barrier at t time, C_{NPs} was the concentration of diosmin in the nanoparticles.

2.8. Cytotoxicity test

CCK-8 assay was used to assess the cytotoxicity of nanoparticles on Caco-2 cells and HT-29 cells. Cells were cultured in Dulbecco's modified Eagle medium (DMEM) for 24 h in 96-well plates. Cells were washed twice with Hank's balanced salt solution (HBSS) before the experiment. Nanoparticle solution was diluted with DMEM. 100 μL of nanoparticle solution at different dilutions (nanoparticle-loaded diosmin concentration of 20 μg/mL) was added to each well and incubated at 37 °C, 5 % CO_2 for 3 h. At the end of incubation, 10 μL of CCK-8 solution was added to each well and incubated for another 1 h. The absorbance was measured by zymography at 450 nm. The absorbance of cells with only DMEM added was used as a blank control group for 100 % cell viability. Each sample was tested in triplicate.

2.9. In vitro antioxidant capacity determination

According to the method of Zhang et al. (Eruygur, Koçyiğit, Taslimi, Ataş, Tekin, & Gülçin, 2019; Gulcin & Alwasel, 2023; Karagecili et al., 2023; Polat Kose et al., 2020; Zhang, Zhou, Zhao, Ning, Sun-Waterhouse, & Sun, 2017), the *in vitro* antioxidant capacity of free diosmin, unloaded nanoparticles and diosmin-loaded nanoparticles was studied, including the determination of $DPPH^+$ and $ABTS^+$ free radical clearance. First, DPPH powder was weighed and dissolved in 95 % ethanol. The sample solution was mixed with 0.2 mM DPPH solution in equal volume. The post-vortex mixture reacted at room temperature in the dark for 30 min, and then the absorbance was measured at 517 nm with a spectrophotometer. The DPPH solution was replaced by ethanol in the blank and the sample solution was replaced by ethanol in the control. Dilute the protein concentration of the test sample to 2 mg/mL. The $DPPH^+$ free radical scavenging activity of the sample was calculated as follows:

$$\text{DPPH}\mathit{free radical clearance}(\%) = \left[1 - \left(A_{sample} - A_{blank}\right)/A_{control}\right]$$

Among them, A_{sample}, A_{blank} and $A_{control}$ are the absorbance of sample, blank and control at 517 nm. In order to ensure the dissolution of diosmin, it was first dissolved in DMSO and then diluted with anhydrous ethanol to the required concentration for subsequent determination.

For the determination of $ABTS^+$ free radical clearance rate, 7 mM ABTS diammonium salt reserve solution and 2.45 mM potassium persulfate reserve solution were mixed and incubated in the dark for 12–16 h. The mixture was diluted 10–20 times with 0.2 M phosphate buffer (pH 7.4) until the absorbance level at 734 nm was 0.70 ± 0.02, which was the $ABTS^+$ free radical working solution. A 50 μL sample was added to 150 μL $ABTS^+$ radical working solution and the absorbance of 734 nm was determined at 6 min. The $ABTS^+$ radical scavenging activity was calculated by substituting a Trolox standard curve of 20–100 μM to convert the Trolox equivalent antioxidant capacity (TEAC, μM TE/g). In order to ensure the dissolution of diosmin, it was first dissolved in DMSO and then diluted with water to the required concentration for subsequent determination.

2.10. Determination of antioxidant capacity of nanoparticles in vivo

To test the antioxidant activity of diosmin *in vivo*, we established a model of acute inflammation induced by intraperitoneal injection of lipopolysaccharide (LPS) (X. Wang et al., 2021; H. Wu et al., 2020). ICR mice (male, 6–8 weeks, 30–35 g) were randomly divided into 7 groups (n = 4 for each group): (1) Control group; (2) LPS group; (3) LPS + free diosmin group; (4) LPS + SPN-D group; (5) LPS + CT-SPN-D group; (6) LPS + HSPN-D group; and (7) LPS + CT-HSPN-D group. Mice were given 0.1 mg/ kg normal saline or 60 μg/kg free diosmin/nanoparticles solution by gavage for 3 days, and then on the fourth day, except foe the Control group, the remaining 6 groups of mice, were intraperitoneally injected with LPS (2.0 mg/kg). All Mice were executed overnight after intraperitoneal injection of LPS. Brains were collected and frozen in liquid nitrogen and kept at −80 °C before utilization.

According to the manufacturer's instructions, the commercial kit (Beyotime Biotechnology Co., Ltd. Shanghai, China) was used to measure the level of malondialdehyde (MDA) in the brain.

2.11. HPLC of diosmin

Diosmin was detected by the HPLC (Essentia LC-16, Shimadzu, Japan) equipped with a reversed-phase C18 column (25 cm × 4.6 mm, particle size = 5 μm). Experimental conditions: mobile phase A: water, mobile phase B: methanol, A: B = 60: 40 (v / v), flow rate: 0.7 mL/min, temperature: 35 °C. The column effluent was monitored by an UV detector at 345 nm. 20 μL of samples were injected into the analytical column automatically at the same time with the mobile phase solutions. The peak area calibration curve versus diosmin concentration in the concentration range of 0–7 μg/mL was Y = 14735.357 X + 2300.367 ($R^2 = 0.999$). The retention time was 26.5 ± 0.3 min.

2.12. Statistics

Data were reported as the mean ± standard deviation (SD). and analyzed with Graph Pad Prism 8.0.2 (Graph Pad Software, San Diego, CA, USA) and IBM SPSS statistics 23 (IBM Corporation, Armonk, NY, USA). One-way analysis of variance was used for comparisons, followed by Tukey post hoc multiple comparison test. $p \leq 0.05$ was regarded as statistical significance.

3. Results and discussion

3.1. Construction and Characterization of nanoparticles

Enzymatic hydrolysis (Shen, Zhou, Zhang, Yuan, Zhao, & Zhao, 2020) and heat treatment (Martinez, Farías, & Pilosof, 2011) have been reported to promote self-assembly of inducible peptide, and heat treatment may influence the characteristics of nanoparticles. Thus, we constructed two types of soybean peptide nanoparticles to load diosmin, the heat-untreated or heat-treated form. The scheme of the nanoparticles was shown in Fig. 1. Diosmin was encapsulated by the self-assemble of soy peptides first and then the nanoparticles were coated with CSK linked TMC to form the bilayer structure. We examined the morphology and appearance of the four kinds of nanoparticles SPN-D, HSPN-D, CT-SPN-D and CT-HSPN-D by TEM. It could be seen in Fig. 2, the nanoparticles SPN-D and HSPN-D were nearly spherical, but the morphology of nanoparticles CT-SPN-D and CT-HSPN-D became extremely irregular with increased particle size, and the nanoparticles tended to gather together. The results indicated that CSK-TMC was successfully covered onto the nanoparticles SPN-D and HSPN-D. The coating of CSK-TMC was mediated by the anionic cross-linking of TPP. When TPP and Tween 80 were added to the mixture solution, the electrostatic interactions were enhanced, which favored CSK-TMC to coat the SPN-D/HSPN-D

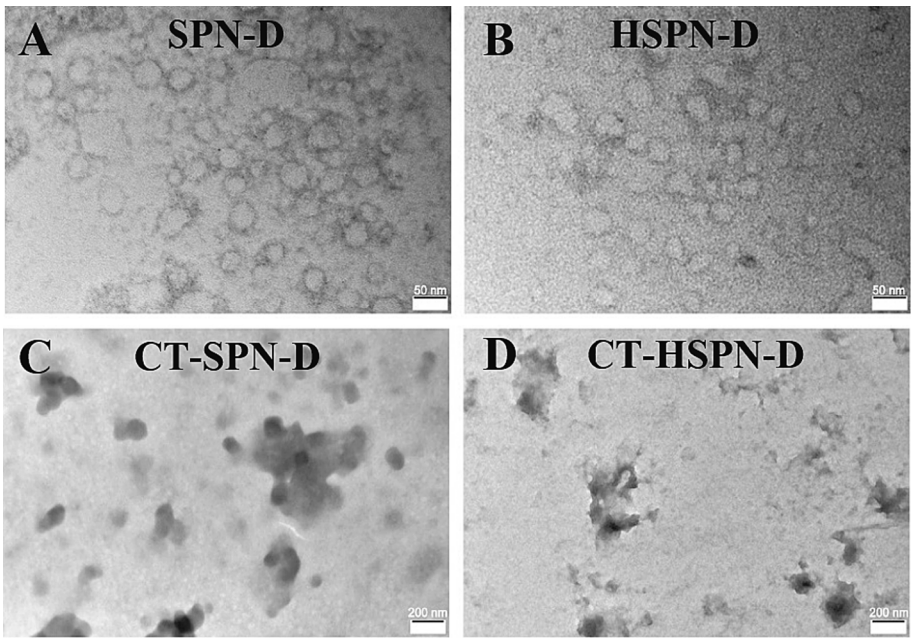

Fig. 2. TEM images of nanoparticles. (A) SPN-D, (B) HSPN-D (the scale bar indicates 50 nm) and (C) CT-SPN-D, (D) CT-HSPN-D (the scale bar indicates 200 nm).

nanoparticles, and thus the particle size increased (de Britto, de Moura, Aouada, Mattoso, & Assis, 2012).

Then, the particle size and zeta potential were examined. Particle size was indicated in Table 1, and the average particle size of SPN-D was smaller than that of HSPN-D. Following CSK-TMC wrapping, the granularity of CT-SPN-D and CT-HSPN-D added. The particle size of CT-SPN-D increased from 93.60 nm to 248.61 nm, and the particle size of CT-HSPN-D increased from 97.72 nm to 253.24 nm. Similarly, the PDI values of both CT-SPN-D and CT-HSPN-D increased, while the homogeneity decreased. This might attribute to the gathering of the nanoparticles as shown in Fig. 2C and D. It was determined and calculated that the encapsulation efficiencies (EE) of SPN-D and HSPN-D were almost 97.01 and 97.28 %, whereas the EE of CT-SPN-D and CT-HSPN-D were reduced to 88.45 and 86.23 %, respectively, after coating with CSK-TMC. The solubility of diosmin in water was reported to be low at about 0.54 μg/mL. In this study, the concentration of loaded diosmin was calculated according to the EE of SPN-D and HSPN-D to be 48.51–48.64 μg/mL, about 90 times higher than the solubility of diosmin in water. However, during the CSK-TMC coating process, the solution of nanoparticles not coated with CSK-TMC was diluted 5 times, so the concentration of loaded diosmin in nanoparticles coated by CSK-TMC was reduced. These results indicated that diosmin was successfully loaded with soy peptides and CSK-TMC to form nanoparticles, and these synthesized nanoparticles could enhance the solubility of diosmin.

Nanoparticles were examined by XRD to determine the crystallinity of diosmin after it was loaded. The XRD patterns of free diosmin and SPN, SPN-D, HSPN, HSPN-D are shown in Fig. 3A. From the figure, the characteristic peaks of diosmin appeared at 12.28, 13.75, 15.69, 19.83, 21.48, 22.54, and 24.09°, which indicated its high crystallinity. These characteristic peak positions were in agreement with the findings of Freag et al (Freag, Elnaggar, & Abdallah, 2013). The diffraction peaks of diosmin-loaded nanoparticles (SPN-D/HSPN-D) and unloaded nanoparticles (SPN /HSPN) were amorphous, and the sharp characteristic peaks of diosmin were completely covered. During the preparation of diosmin nanoparticles, diosmin was first dissolved in alkaline solution, and then the pH of the mixture was adjusted to neutral, during which salts would be generated. The peak at 31.8° may be the crystallization peak of salt formed by acid-base neutralization during the preparation of nanoparticles (Mou, Chen, Wan, Xu, & Yang, 2011). These results showed that diosmin was successfully loaded by SPN/HSPN by changing the crystalline state from crystalline to amorphous.

From the FTIR spectra of Fig. 3B, the typical and prominent peaks of diosmin disappeared during the formation of nanoparticles SPN-D and HSPN-D, which again proved that diosmin was successfully encapsulated into nanoparticles. The peak at 3532 cm^{-1} represents the O—H stretching vibration. From the FTIR spectra of Fig. 3B, by comparing the unloaded diosmin nanoparticles SPN/HSPN with the loaded diosmin nanoparticles SPN-D/HSPN-D, we found that the absorption peak for the hydrogen bonding of soybean peptides at 3450 cm^{-1}/3439 cm^{-1} in the nanoparticles loaded with diosmin was redshifted to 3415 cm^{-1}. This indicated that it formed new hydrogen bonds between diosmin and soybean peptides during the formation of nanoparticles. According to previous research, the hydroxyl groups contained in polyphenols can combine with the amide groups in proteins to form hydrogen bonds, so the new hydrogen bonds in the nanoparticles may be generated of the hydroxyl groups contained in diosmin and the amide groups in soybean peptides (He, Guan, Song, Li, & Huang, 2020).

DSC detection of nanoparticles can be used to study the physical state

Table 1
Particle size and zeta potential of nanoparticle (n = 3, Mean ± SD).

	Particle size (nm)	PDI	Zeta potential (mV)	EE (%)	$C_{diosmin}$ (μg/mL)
Free diosmin	–	–	–	–	0.54 ^{a}
SPN-D	93.60 ± 0.49^{a}	0.188 ± 0.01^{a}	−25.10 ± 0.70^{a}	97.01 ± 0.53 ^{a}	48.51 ± 0.22^{b}
HSPN-D	97.72 ± 0.53^{b}	0.198 ± 0.01^{a}	−25.57 ± 0.49^{a}	97.28 ± 0.44 ^{a}	48.64 ± 0.18^{b}
CT-SPN-D	248.61 ± 1.30^{c}	0.332 ± 0.01^{b}	15.24 ± 0.51^{b}	88.45 ± 0.32^{b}	8.58 ± 0.03^{c}
CT-HSPN-D	253.24 ± 1.61^{d}	0.329 ± 0.01^{b}	12.95 ± 0.67^{c}	86.23 ± 0.48^{c}	8.39 ± 0.04^{c}

PDI, polydispersity index; EE, encapsulation efficiency; $C_{diosmin}$, concentration of encapsulated diosmin. Different letters in the same column indicate significant difference ($P < 0.05$).

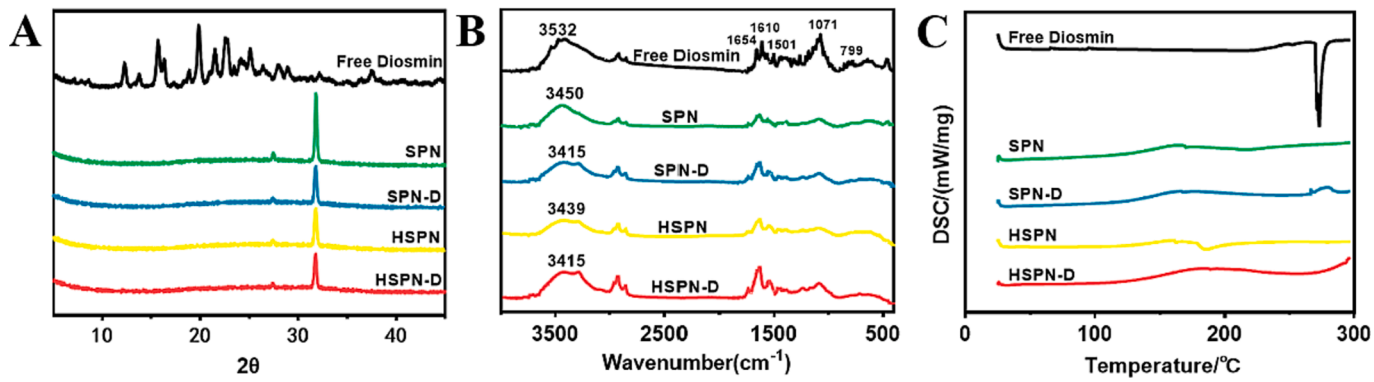

Fig. 3. Characterization of nanoparticles. (A) XRD patterns (B) FT-IR spectra and (C) DSC patterns of free diosmin and nanoparticles (SPN, SPN-D, HSPN, HSPN-D).

of carrier polymers and drugs. From the DSC thermogram of Fig. 3C, free diosmin in a single melting point 273 °C presented as a single endothermic peak, whereas the nanoparticles SPN-D/HSPN-D/CT-SPN-D/CT-HSPN-D loaded with diosmin did not have peaks near this temperature, which indicated that after encapsulation, the crystal morphology of diosmin was changed. This result was in agreement with the XRD analysis in Fig. 3A, which further proved that diosmin in the nanoparticles had been converted from crystalline to amorphous state. All of the above results proved that diosmin could be successfully encapsulated by soybean peptides to form nanoparticles, and instead of ordinary physical mixing, a complex was formed.

The stability of the nanoparticles was determined after storing for 1 day and 16 days at different pH. From Fig. 4A, it could be observed that the zeta potential of SPN-D remained stable at pH 7 and pH 8, but slightly decreased at pH 9. However, the zeta potential of HSPN-D decreased after storing for 16 days at all pH (Fig. 4B). But it could be observed that the value of zeta potential of HSPN-D was higher than that of SPN-D. Zeta potential is the electrical potential that is attached to the boundary of the surrounding liquid layer on the moving particles in the medium. It is a key parameter widely used to predict the stability of suspensions. The higher the value, the more stable the suspension, the more stable of the nanoparticles (L. Wu, Zhang, & Watanabe, 2011). Even after storing for 16 days, all the values of zeta potential were higher than 20 mV, and even higher than 30 mV at pH 9. These results suggested that the nanoparticles possessed favorable stability, especially in alkaline solution, and SPN-D was more stable than HSPN-D.

In order to determine the interaction forces for the nanoparticles loaded with diosmin to maintain stability, experiments were carried out by homogeneously dispersing the nanoparticles SPN-D and HSPN-D in various types of organic solvents, and the average particle size was employed as an evaluation metric. SDS destroyed hydrophobic interactions, urea breaks hydrogen bonds, and DTT interrupts intermolecular disulfide bonds (Ren, Tang, Zhang, & Guo, 2009). In addition to this, SDS disrupts the hydrogen bonds and secondary and tertiary structures within the protein molecules, causing the proteins to lose their natural state of charge and bind to the SDS molecules in a certain

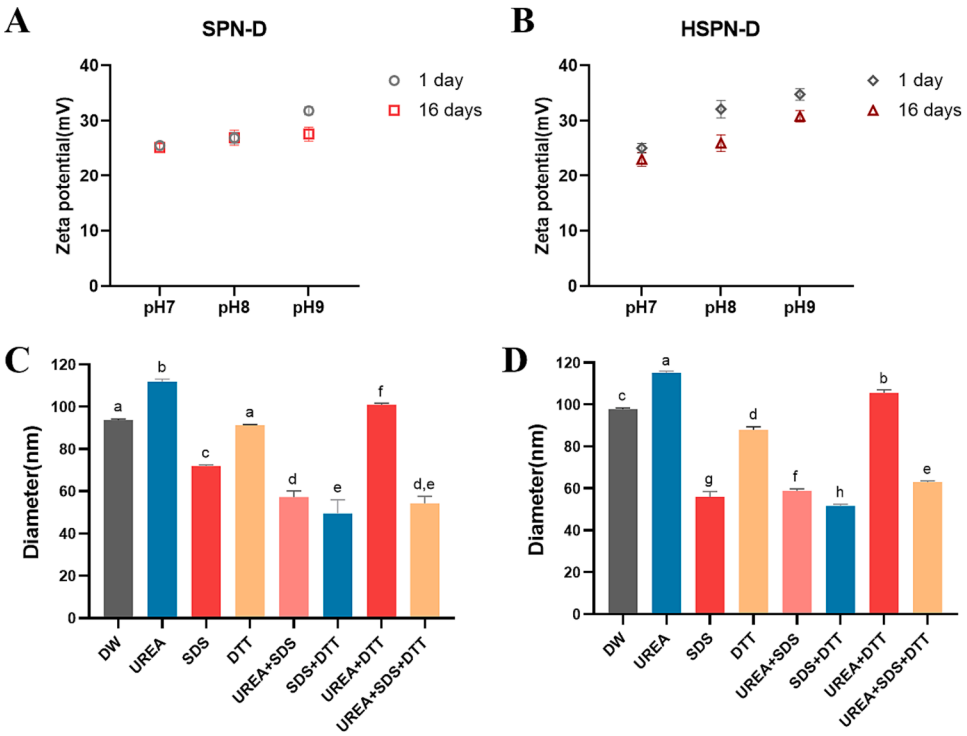

Fig. 4. Stability of the nanoparticles. (A) Zeta potential of SPN-D after storing for 1 day and 16 days. (B) Zeta potential of HSPN-D after storing for 1 day and 16 days. (C) Influence of various protein-perturbing solvents on the average diameter of SPN-D. (D) Influence of various protein-perturbing solvents on the average diameter of HSPN-D. DW refers to distilled water. Different letters (a, b, c) on each column indicate significant difference ($p < 0.05$).

ratio to form SDS-protein complexes with a large number of negative charges, which increases the negative charge and causes static repulsion. The results were shown in Fig. 4C and D. From the findings of SPN-D in Fig. 4C, we saw that the structure of nanoparticles was highly susceptible to the action of 0.5 % SDS and 6 M urea alone or in combination, but resistant to the presence of possibly 30 mM DTT alone. From the results of Fig. 4D, the nanoparticles HSPN-D formed from soybean peptides after heat treatment, its structure was not only affected by 0.5 % SDS and 6 M urea, but also sensitive to 30 mM DTT. According to findings, the stability of nanoparticles SPN-D was mainly maintained by hydrogen bonding and hydrophobic function of noncovalent interaction, while the stability of HSPN-D was maintained by noncovalent interactions as well as disulfide bonding, which showed that some properties of soy peptides were changed after heat treatment.

3.2. Gastric stability and bioaccessibility of nanoparticles

As the nanoparticles moved through the gastrointestinal tract, they may be attacked by enzymes or acids in body fluids (Vitulo et al., 2022). The stability of nanoparticles in the gastrointestinal tract was assessed by determining the concentration of released free diosmin. Results suggested that the release of diosmin in SPN-D or HSPN-D was a little higher than free diosmin in imitating stomach digestion, while the release of diosmin in CT-SPN-D or CT-HSPN-D wasn't detected (Fig. 5A). But in the simulated gastrointestinal digestion, the release rates of the four nanoparticle groups were significantly higher than the free diosmin group. These results indicated that the nanoparticles could protect diosmin against gastric digestion but increase the release of diosmin in intestinal digestion. TMC has good solubility under neutral pH, and neutral and alkaline pH environments could enhance the permeability and absorption properties of TMC (Chen, Svirskis, Lu, Ying, Huang, & Wen, 2018). This might help to explain the un-detection of diosmin of CT-SPN-D and CT-HSPN-D groups in simulate gastric digestion but increased release of diosmin in simulate gastrointestinal digestion.

The bioaccessiblity of the nanoparticles loaded with diosmin was determined by measuring the concentration of diosmin released from the nanoparticles crossing the intestinal barrier. As shown in Fig. 5B, the permeability curve of free diosmin and nanoparticles absorbed through the intestine showed that the permeability of free diosmin was less than 5 %, while the permeability of the nanoparticle groups loaded with diosmin was much higher than that of free diosmin group, thus significantly improving the intestinal permeation of diosmin ($p < 0.01$). Compared with 4.47 ± 1.07 % for free diosmin, the bioaccessibility of diosmin of CT-SPN-D reached to 53.74 ± 5.52 % in small intestine. To summarize the results, it was stated that the bioaccessibility of diosmin was improved by SPN and HSPN, and the nanoparticles were further promoted by the encapsulation of CSK-TMC. As the bioaccessibility of nutrients is largely depends on the water solubility, the increased bioaccessibility of nanoparticle-loaded diosmin attributed to the increased water solubility after embedding. The results were consistent with the studies of Zhang et al, which reported that the encapsulation of curcumin by soy peptides significantly increased the bioaccessibility of curcumin (Zhang, Yuan, Shen, Zhou, Zhao, & Zhao, 2021). In addition, previous research has shown that TMC expands at intestinal pH to release encapsulated goods (Ling, Wu, Neish, & Champion, 2019), this may also contribute to the increased bioaccessibility of diosmin in CSK-TMC coated groups.

3.3. Cytotoxicity assessment of nanoparticles

Security of nanoparticles was assessed using the CCK-8 method for evaluating the toxicity of nanoparticles on the cell viability of Caco-2 cells and HT-29 cells. According to the experimental results in Fig. 6, the cell viability of Caco-2 cells and HT-29 cells co-incubated with nanoparticles for 3 h was above 85 %. The cell survival rates of nanoparticles after CSK-TMC encapsulation were higher than those of unencapsulated nanoparticles, even higher than 100 %. According to previous studies, TMC does not change cell morphology or viability, low-dose TMC even promotes the growth of human fibroblast cells (Abueva et al., 2021). Therefore, the nanoparticle drug delivery system was secure and harmless.

3.4. Antioxidant capacity

The free radical scavenge activity of the nanoparticles was measured to test whether the antioxidant activity of diosmin was improved. As shown in Fig. 7A, there was almost no $DPPH^+$ free radicals scavenge ability of diosmin, which attributed to the low water solubility. After embedding by nanoparticles, the $DPPH^+$ free radicals scavenge rate reached to about 80 %. However, it was not negligible that SPN and HSPN also possessed high $DPPH^+$ free radicals scavenge activity. The $ABTS^+$ scavenge activity was similar to $DPPH^+$ (Fig. 7B). The $ABST^+$ scavenge rate of nanoparticles groups was far more than that of free diosmin group.

It has been reported that diosmin could alleviate LPS - induced brain oxidative stress (Zhao, Zhang, Zhang, Wang, Chen, & Shao, 2024). To determine the contribution of the nanoparticles on the antioxidant activity of diosmin *in vivo*, the mice model of oxidative stress induced by LPS was employed. The level of brain MDA was determined after oral administration of free diosmin or nanoparticles. MDA is a metabolite of lipid peroxidation in living organisms, and its level can reflect the level of oxidative stress (Dong, Li, Zhen, Wang, Shao, & Luo, 2013). From Fig. 7C, it was observed that the level of MDA was significantly increased in LPS group but obviously decreased in the bilayer nanoparticles groups (Fig. 7C). In previous studies (Zhao et al., 2024), the administration of diosmin was 50 mg/kg, but here in this study, the treating dosage of diosmin was only 60 μg/kg. This indicated that the bioavailability of diosimin was dramatically increased after

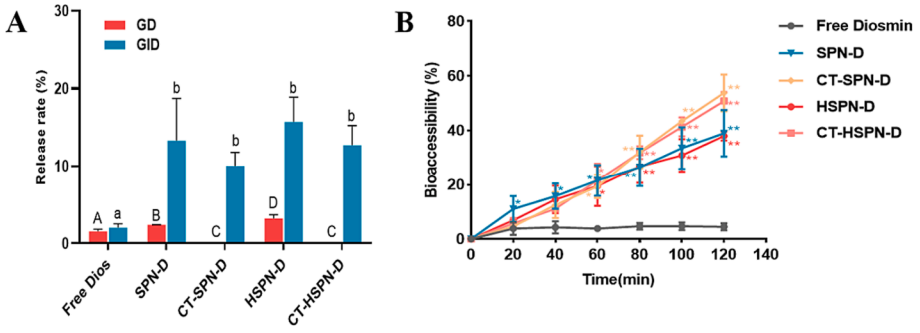

Fig. 5. Gastrointestinal stability and bioaccessibility of nanoparticles. (A) The release of free diosmin and nanoparticles in simulated gastric and intestinal fluid. The different letters on each column (A, B, C for GD and a, b, c for GID) indicate significant difference ($p < 0.05$). (B) bioaccessibility of free diosmin and diosmin-loaded nanoparticles (SPN-D, CT-SPN-D and HSPN-D, CT-HSPN-D). *$p < 0.05$ and **$p < 0.01$ vs. free diosmin.

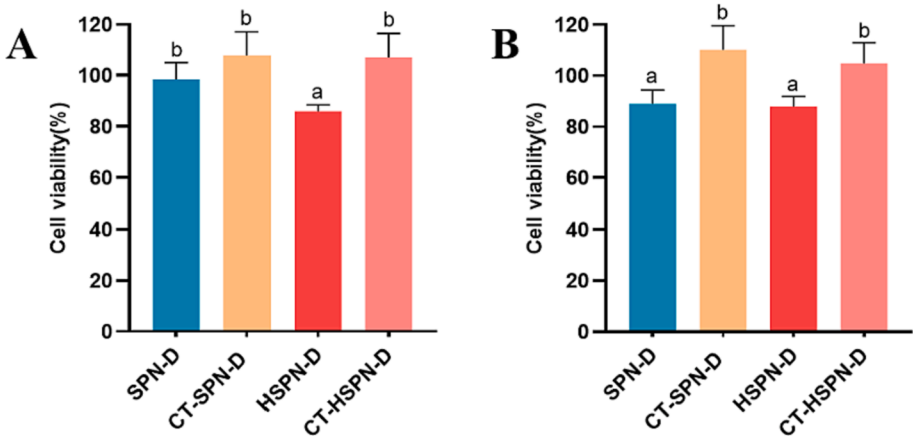

Fig. 6. Effects of diosmin loaded nanoparticles on the viability of Caco-2 cells (A) and HT-29 (B) (Mean ± SD, n = 5). Different letters (a, b, c) on each column indicate significant difference ($p < 0.05$).

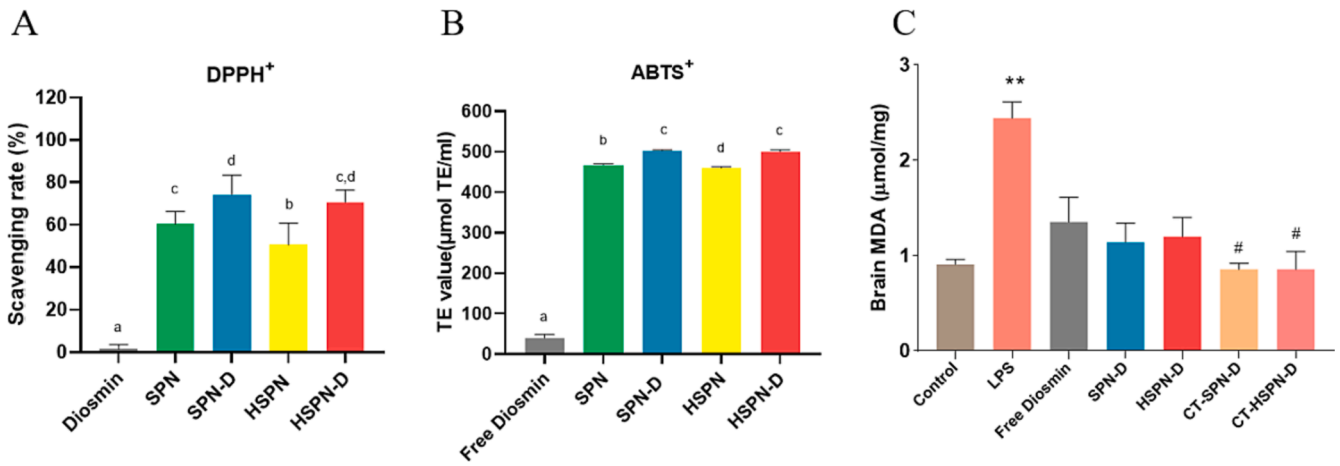

Fig. 7. Antioxidant activities of free diosmin and diosmin-loaded nanoparticles. (A) $DPPH^+$ scavenging rate. (B) $ABTS^+$ scavenging activity. (C) MDA level in brain. *$p < 0.05$ vs. Control, #$p < 0.05$ vs. free diosmin.

encapsulated by the bilayer nanoparticles. However, the effect of single layer ones was not significant, which was consistent with the results of Fig. 5B that the bioaccessibility of the bilayer nanoparticles was higher than single layer ones. Together, those results indicated that nanoparticles greatly enhanced the antioxidant activity of diosmin either *in vitro* or *in vivo*.

According to previous study, diosmin could cross the blood–brain barrier (BBB) (Chang et al., 2021). In this study, the outer CSK-TMC layer could help the nanoparticles cross the intestinal barrier, and then the inner SPN-D/HSPN-D enter into the blood. However, whether SPN-D or HSPN-D release diosmin in the blood or could cross the BBB to release disomin needs to be investigate further.

4. Conclusion

In this study, the bilayer nanoparticles with the inner layer formed by the self-assembly of soy peptides and the outer layer formed by CSK coupled TMC were fabricated to encapsulate diosmin. The bilayer nanoparticles increased the water solubility of diosmin and were stable during storage and in the gastrointestinal environment. They could protect diosmin against gastric digestion but release diosmin in intestinal digestion, and significantly improve the bioaccessibility diosmin. *In vitro* and *in vivo* studies showed that encapsulated diosmin presented better antioxidant activity. The present research provided theoretical support and potential solution for improving oral bioavailability of bioactive compounds.

Informed consent statement

Not applicable.

Funding sources

This work was supported by the National Key R&D Program of China [No. 2022YFF1100104] and the National Natural Science Foundation of China [No. 31901609].

CRediT authorship contribution statement

Sen Li: Writing – review & editing, Methodology, Conceptualization. **Tong Guan:** Writing – original draft, Data curation. **Hongyan Lv:** Formal analysis, Data curation. **Yuwei Cai:** Formal analysis. **Wanqing Cao:** Validation. **Ze Zhang:** Validation. **Hongdong Song:** Methodology. **Hongwei Cao:** Software. **Xiao Guan:** Writing – review & editing, Supervision.

Declaration of competing interest

The authors declare that they have no known competing financial interests or personal relationships that could have appeared to influence

the work reported in this paper.

Data availability

Data will be made available on request.

References

Abd El Hady, W. E., Mohamed, E. A., Soliman, O.-A.-E.-A., & El-Sabbagh, H. M. (2019). In vitro–in vivo evaluation of chitosan-PLGA nanoparticles for potentiated gastric retention and anti-ulcer activity of diosmin. *International Journal of Nanomedicine, 14* (null), 7191–7213. https://doi.org/10.2147/IJN.S213836

Abueva, C., Ryu, H. S., Min, J. W., Chung, P. S., You, H. S., Yang, M. S., & Woo, S. H. (2021). Quaternary ammonium N, N, N-trimethyl chitosan derivative and povidone-iodine complex as a potent antiseptic with enhanced wound healing property. *International Journal of Biological Macromolecules, 182*, 1713–1723. https://doi.org/10.1016/j.ijbiomac.2021.05.153

Anwer, M. K., Ahmed, M. M., Alshetaili, A., Almutairy, B. K., Alalaiwe, A., Fatima, F., & Iqbal, M. (2020). Preparation of spray dried amorphous solid dispersion of diosmin in soluplus with improved hepato-renoprotective activity: In vitro anti-oxidant and in-vivo safety studies. *Journal of Drug Delivery Science and Technology, 60*, Article 102101. https://doi.org/10.1016/j.jddst.2020.102101

Berkoz, M. (2019). Diosmin suppresses the proinflammatory mediators in lipopolysaccharide-induced RAW264.7 macrophages via NF-κB and MAPKs signal pathways. *General Physiology and Biophysics, 38*(4), 315–324. https://doi.org/10.4149/gpb_2019010

Campos-Vega, R., Vázquez-Sánchez, K., López-Barrera, D., Loarca-Piña, G., Mendoza-Díaz, S., & Oomah, B. D. (2015). Simulated gastrointestinal digestion and in vitro colonic fermentation of spent coffee (Coffea arabica L.): Bioaccessibility and intestinal permeability. *Food Research International, 77*, 156–161. https://doi.org/10.1016/j.foodres.2015.07.024

Carballo-Villalobos, A. I., González-Trujano, M. E., Pellicer, F., Alvarado-Vásquez, N., & López-Muñoz, F. J. (2018). Central and peripheral anti-hyperalgesic effects of diosmin in a neuropathic pain model in rats. *Biomedicine & Pharmacotherapy, 97*, 310–320. https://doi.org/10.1016/j.biopha.2017.10.077

Chang, Y. L., Li, Y. F., Chou, C. H., Huang, L. C., Wu, Y. P., Kao, Y., & Tsai, C. K. (2021). Diosmin Inhibits Glioblastoma Growth through Inhibition of Autophagic Flux. *International Journal of Molecular Sciences, 22*(19). https://doi.org/10.3390/ijms221910453

Chen, G., Svirskis, D., Lu, W., Ying, M., Huang, Y., & Wen, J. (2018). N-trimethyl chitosan nanoparticles and CSKSSDYQC peptide: N-trimethyl chitosan conjugates enhance the oral bioavailability of gemcitabine to treat breast cancer. *Journal Of Controlled Release, 277*, 142–153.

de Britto, D., de Moura, M. R., Aouada, F. A., Mattoso, L. H. C., & Assis, O. B. G. (2012). N, N, N-trimethyl chitosan nanoparticles as a vitamin carrier system. *Food Hydrocolloids, 27*(2), 487–493. https://doi.org/10.1016/j.foodhyd.2011.09.002

Dong, L. Y., Li, S., Zhen, Y. L., Wang, Y. N., Shao, X., & Luo, Z. G. (2013). Cardioprotection of vitexin on myocardial ischemia/reperfusion injury in rat via regulating inflammatory cytokines and MAPK pathway. *The American Journal of Chinese Medicine, 41*(6), 1251–1266. https://doi.org/10.1142/S0192415X13500845

Eruygur, N., Koçyiğit, U. M., Taslimi, P., Ataş, M., Tekin, M., & Gülçin, İ. (2019). Screening the in vitro antioxidant, antimicrobial, anticholinesterase, antidiabetic activities of endemic Achillea cucullata (Asteraceae) ethanol extract. *South African Journal of Botany, 120*, 141–145. https://doi.org/10.1016/j.sajb.2018.04.001

Freag, M. S., Elnaggar, Y. S., & Abdallah, O. Y. (2013). Development of novel polymer-stabilized diosmin nanosuspensions: In vitro appraisal and ex vivo permeation. *International Journal of Pharmaceutics, 454*(1), 462–471. https://doi.org/10.1016/j.ijpharm.2013.06.039

Freag, M. S., Elnaggar, Y. S. R., & Abdallah, O. Y. (2013). Lyophilized phytosomal nanocarriers as platforms for enhanced diosmin delivery: Optimization and ex vivo permeation. *International Journal of Nanomedicine, 8*(null), 2385–2397. https://doi.org/10.2147/IJN.S45231

Garner, R., Garner, J., Gregory, S., Whattam, M., Calam, A., & Leong, D. (2002). Comparison of the Absorption of Micronized (Daflon 500® mg) and Nonmicronized 14C-diosmin Tablets After Oral Administration to Healthy Volunteers by Accelerator Mass Spectrometry and Liquid Scintillation Counting. *Journal of pharmaceutical sciences, 91*(1), 32–40.

Gulcin, İ., & Alwasel, S. H. (2023). DPPH Radical Scavenging Assay. *Processes, 11*(8), 2248. https://www.mdpi.com/2227-9717/11/8/2248.

He, A., Guan, X., Song, H., Li, S., & Huang, K. (2020). Encapsulation of (−)-epigallocatechin-gallate (EGCG) in hordein nanoparticles. *Food Bioscience, 37*. https://doi.org/10.1016/j.fbio.2020.100727

Hsu, C. C., Lin, M. H., Cheng, J. T., & Wu, M. C. (2017). Diosmin, a Citrus Nutrient, Activates Imidazoline Receptors to Alleviate Blood Glucose and Lipids in Type 1-Like Diabetic Rats. *Nutrients, 9*(7). https://doi.org/10.3390/nu9070684

Karagecili, H., Yılmaz, M. A., Ertürk, A., Kiziltas, H., Güven, L., Alwasel, S. H., & Gulcin, İ. (2023). Comprehensive Metabolite Profiling of Berdav Propolis Using LC-MS/MS: Determination of Antioxidant, Anticholinergic, Antiglaucoma, and Antidiabetic Effects. *Molecules, 28*(4), 1739. https://www.mdpi.com/1420-3049/28/4/1739.

Li, S., Lv, H., Chen, Y., Song, H., Zhang, Y., Wang, S., & Guan, X. (2022). N-trimethyl chitosan coated targeting nanoparticles improve the oral bioavailability and antioxidant activity of vitexin. *Carbohydrate Polymers, 286*, Article 119273.

Ling, K., Wu, H., Neish, A. S., & Champion, J. A. (2019). Alginate/chitosan microparticles for gastric passage and intestinal release of therapeutic protein nanoparticles. *Journal Of Controlled Release, 295*, 174–186.

Liu, F., & Tang, C. H. (2014). Emulsifying properties of soy protein nanoparticles: Influence of the protein concentration and/or emulsification process. *Journal of Agricultural and Food Chemistry, 62*(12), 2644–2654. https://doi.org/10.1021/jf405348k

Martinez, M. J., Farías, M. E., & Pilosof, A. M. R. (2011). Casein glycomacropeptide pH-driven self-assembly and gelation upon heating. *Food Hydrocolloids, 25*(5), 860–867. https://doi.org/10.1016/j.foodhyd.2010.08.005

Moriwaki, M., Kito, K., Nakagawa, R., Kapoor, M. P., Matsumiya, Y., Fukuhara, T., & Kuroiwa, Y. (2023). Increased bioavailability of diosmetin-7-glucoside-γ-cyclodextrin inclusion complex compared with diosmin in Sprague-Dawley rats. *Bioscience, biotechnology, and biochemistry, 87*(7), 771–776. https://doi.org/10.1093/bbb/zbad051

Mou, D., Chen, H., Wan, J., Xu, H., & Yang, X. (2011). Potent dried drug nanosuspensions for oral bioavailability enhancement of poorly soluble drugs with pH-dependent solubility. *International Journal of Pharmaceutics, 413*(1–2), 237–244. https://doi.org/10.1016/j.ijpharm.2011.04.034

Naso, L., Martínez, V. R., Lezama, L., Salado, C., Valcarcel, M., Ferrer, E. G., & Williams, P. A. M. (2016). Antioxidant, anticancer activities and mechanistic studies of the flavone glycoside diosmin and its oxidovanadium(IV) complex. Interactions with bovine serum albumin. *Bioorganic & Medicinal Chemistry, 24*(18), 4108–4119. https://doi.org/10.1016/j.bmc.2016.06.053

Om, H., El-Naggar, M. E., El-Banna, M., Fouda, M. M. G., Othman, S. I., Allam, A. A., & Morsy, O. M. (2020). Combating atherosclerosis with targeted Diosmin nanoparticles-treated experimental diabetes. *Investigational New Drugs, 38*(5), 1303–1315. https://doi.org/10.1007/s10637-020-00905-6

Paredes, M. D., Romecín, P., Atucha, N. M., O'Valle, F., Castillo, J., Ortiz, M. C., & García-Estañ, J. (2018). Beneficial Effects of Different Flavonoids on Vascular and Renal Function in L-NAME Hypertensive Rats. *Nutrients, 10*(4). https://doi.org/10.3390/nu10040484

Polat Kose, L., Bingol, Z., Kaya, R., Goren, A. C., Akincioglu, H., Durmaz, L., & Gülçin, İ. (2020). Anticholinergic and antioxidant activities of avocado (Folium perseae) leaves – phytochemical content by LC-MS/MS analysis. *International Journal of Food Properties, 23*(1), 878–893. https://doi.org/10.1080/10942912.2020.1761829

Pushkaran, A. C., Vinod, V., Vanuopadath, M., Nair, S. S., Nair, S. V., Vasudevan, A. K., & Mohan, C. G. (2019). Combination of Repurposed Drug Diosmin with Amoxicillin-Clavulanic acid Causes Synergistic Inhibition of Mycobacterial Growth. *Scientific Reports, 9*(1), 6800. https://doi.org/10.1038/s41598-019-43201-x

Ren, C., Tang, L., Zhang, M., & Guo, S. (2009). Structural characterization of heat-induced protein particles in soy milk. *Journal of Agricultural and Food Chemistry, 57*, 1921–1926.

Russo, R., Chandradhara, D., & De Tommasi, N. (2018). Comparative Bioavailability of Two Diosmin Formulations after Oral Administration to Healthy Volunteers. *Molecules, 23*(9), 2174. https://www.mdpi.com/1420-3049/23/9/2174.

Russo, R., Mancinelli, A., Ciccone, M., Terruzzi, F., Pisano, C., & Severino, L. (2015). Pharmacokinetic profile of μSMIN Plus™, a new micronized diosmin formulation, after oral administration in rats. *Natural Product Communications, 10*(9), 1569–1572. http://europepmc.org/abstract/MED/26594761.

Serra, R., Ielapi, N., Bitonti, A., Candido, S., Fregola, S., Gallo, A., & Gallelli, L. (2021). Efficacy of a low-dose diosmin therapy on improving symptoms and quality of life in patients with chronic venous disease: randomized, double-blind, Placebo-Controlled Trial. *Nutrients, 13*(3), 999. https://www.mdpi.com/2072-6643/13/3/999.

Shen, P., Zhou, F., Zhang, Y., Yuan, D., Zhao, Q., & Zhao, M. (2020). Formation and characterization of soy protein nanoparticles by controlled partial enzymatic hydrolysis. *Food Hydrocolloids, 105*. https://doi.org/10.1016/j.foodhyd.2020.105844

Vitulo, M., Gnodi, E., Meneveri, R., & Barisani, D. (2022). Interactions between nanoparticles and intestine. *International Journal of Molecular Sciences, 23*(8), 4339. https://www.mdpi.com/1422-0067/23/8/4339.

Vrbata, P., Berka, P., Stránská, D., Doležal, P., & Lázníček, M. (2014). Electrospinning of diosmin from aqueous solutions for improved dissolution and oral absorption. *International Journal of Pharmaceutics, 473*(1), 407–413. https://doi.org/10.1016/j.ijpharm.2014.07.017

Wang, X., Wang, L., Dong, R., Huang, K., Wang, C., Gu, J., & Meng, Q. (2021). Luteolin ameliorates LPS-induced acute liver injury by inhibiting TXNIP-NLRP3 inflammasome in mice. *Phytomedicine, 87*, Article 153586. https://doi.org/10.1016/j.phymed.2021.153586

Wang, Y. C., Li, P. W., & Kong, L. X. (2013). Chitosan-Modified PLGA Nanoparticles with Versatile Surface for Improved Drug Delivery. *AAPS PharmSciTech, 14*(2), 585–592. https://doi.org/10.1208/s12249-013-9943-3

Wojnar, W., Kaczmarczyk-Sedlak, I., & Zych, M. (2017). Diosmin ameliorates the effects of oxidative stress in lenses of streptozotocin-induced type 1 diabetic rats. *Pharmacological Reports, 69*(5), 995–1000. https://doi.org/10.1016/j.pharep.2017.04.005

Wu, H., Wang, Y., Zhang, Y., Xu, F., Chen, J., Duan, L., & Zhang, F. (2020). Breaking the vicious loop between inflammation, oxidative stress and coagulation, a novel anti-thrombus insight of nattokinase by inhibiting LPS-induced inflammation and oxidative stress. *Redox Biology, 32*, Article 101500. https://doi.org/10.1016/j.redox.2020.101500

Wu, L., Zhang, J., & Watanabe, W. (2011). Physical and chemical stability of drug nanoparticles. *Advanced Drug Delivery Reviews, 63*(6), 456–469. https://doi.org/10.1016/j.addr.2011.02.001

Zhang, Y., Yuan, D., Shen, P., Zhou, F., Zhao, Q., & Zhao, M. (2021). pH-Driven formation of soy peptide nanoparticles from insoluble peptide aggregates and their

application for hydrophobic active cargo delivery. *Food Chemistry, 355*, Article 129509.

Zhang, Y., Zhou, F., Zhao, M., Lin, L., Ning, Z., & Sun, B. (2018). Soy peptide nanoparticles by ultrasound-induced self-assembly of large peptide aggregates and their role on emulsion stability. *Food Hydrocolloids, 74*, 62–71. https://doi.org/10.1016/j.foodhyd.2017.07.021

Zhang, Y., Zhou, F., Zhao, M., Ning, Z., Sun-Waterhouse, D., & Sun, B. (2017). Soy peptide aggregates formed during hydrolysis reduced protein extraction without decreasing their nutritional value. *Food & Function, 8*(12), 4384–4395.

Zhao, J., Zhang, M., Zhang, H., Wang, Y., Chen, B., & Shao, J. (2024). Diosmin ameliorates LPS-induced depression-like behaviors in mice: Inhibition of inflammation and oxidative stress in the prefrontal cortex. *Brain Research Bulletin, 206*, Article 110843. https://doi.org/10.1016/j.brainresbull.2023.110843